Chapter 2

Experimental Procedures

2.1 Introduction

This chapter introduces the experimental procedures utilised to characterise austempered ductile irons obtained in the present thesis. The experiments here described were also used to validate models included in latter chapters. Fig. 2.1 is the general flow chart of experimental procedures.

2.2 Material

A ductile cast iron produced in a commercial foundry using electric melting has been used for the experiments. Its chemical composition is Fe-3.55C-2.5Si-0.55Mn-0.15Mo-0.31Cu-0.042Mg wt%. Solid cylindrical specimens with dimensions 8 mm diameter and 12 mm length were machined from a keel block for heat treatments.

2.3 Heat treatments

2.3.1 Furnace heat treatments

All samples which required heat treatment in furnace, either for homogenisation or for austempering treatment, were sealed in quartz tubes under a partial pressure of argon to prevent oxidation. Homogenisation consisted in holding the samples at 1000°C for 3 days

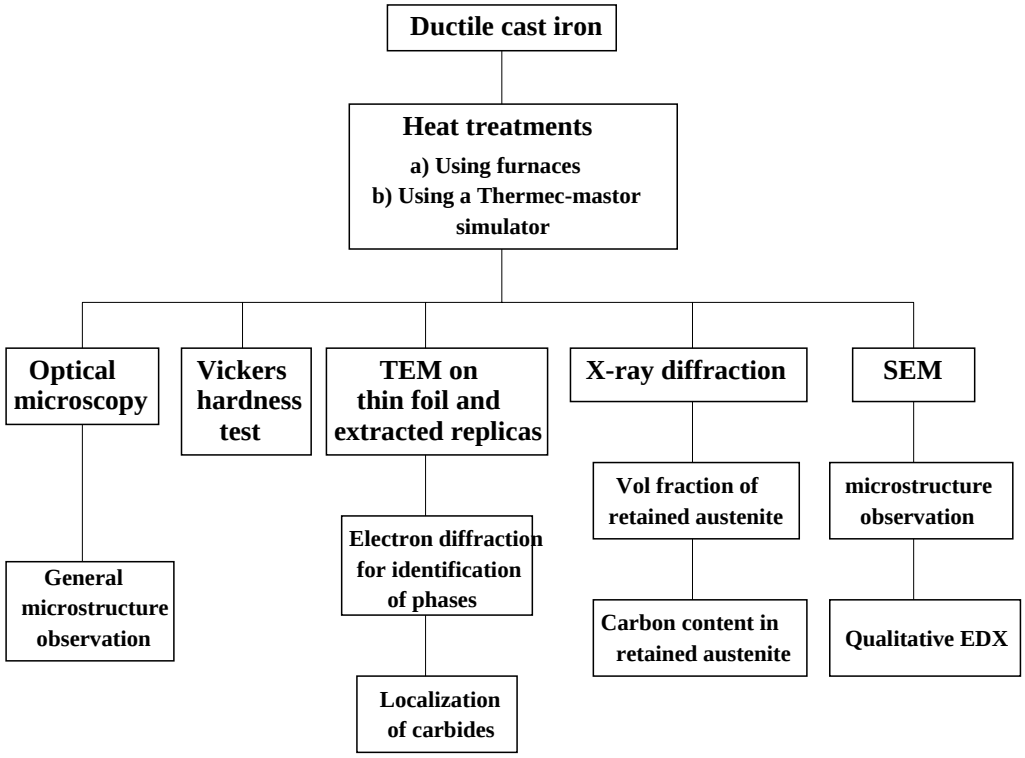

Figure 2.1: Flow chart illustrating the experimental programme for austempered samples.

before quenching in water with breaking silica tubes. Calibration of furnaces was verified before any heat treatment was performed to ensure accuracy of temperatures.

2.3.2 Thermomechanical simulator heat treatments

The "Thermecmastor Z" thermomechanical simulator, manufactured by Fuji Electronic Industrial Co. Ltd., is a laboratory machine capable of implementing specified thermal cycles on small samples, under accurate computer control. The temperature and diametrical dilatation of the specimen are measured and thus the progress of phase transformations within the material can be followed.

A solid cylindrical specimen with dimensions of 8 mm diameter and 12 mm length is placed vertically in the chamber (Fig. 2.2) between two silicon nitride dies. The die holders are insulated from the dies by two mica discs. The upper die can be raised and lowered using a hydraulic ram to hold the sample in position. A platinum / platinum-10% rhodium thermocouple is spot-welded to the specimen in a central position with the wires spaced approximately 1 mm apart. The accuracy of the temperature reading is $\pm 3°$ whilst the variation along the specimen length is no more than $\pm 10°$. The diametrical dilatation of the sample is monitored using a He-Ne laser beam, which moves and scans with the ram to ensure the same location on the sample is measured throughout the experiment. The beam is positioned at the same height as the thermocouple on the sample to ensure

that the temperature and dilatation measurements are for the same location.

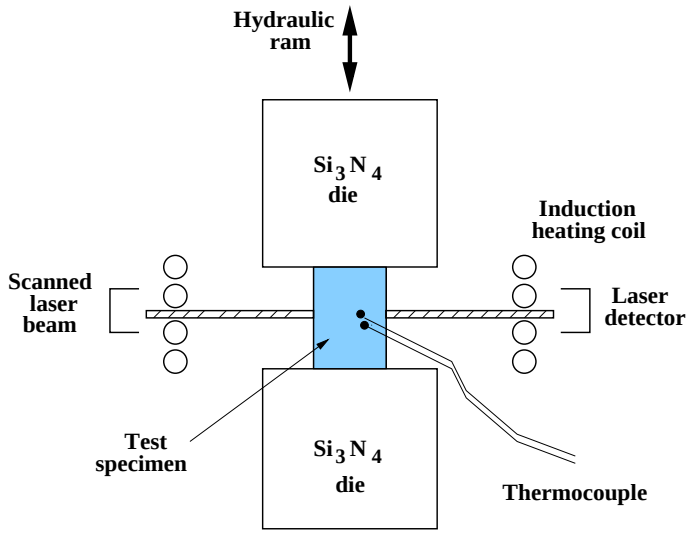

Figure 2.2: The arrangement of equipment within the *Termecmastor Z* thermomechanical simulator. The specimen is situated between Si_3N_4 dies, inside an induction coil. Simultaneous temperature, dilatometric and load data can be measured.

The accuracy of the dilatation reading is $\pm$ 1 μm. The sealed chamber is then pumped out to a vacuum of $\approx 10^{-2}$ Pa to prevent oxidation of the specimen. An inert gas (argon) atmosphere can also be introduced if required. Heating is provided by a water-cooled, high frequency induction coil which surrounds the sample. Cooling can be controlled using gas (He or N_2) or water. Helium was used in all the experiments. Time, temperature and dilatation are recorded and can be stored on a computer for subsequent analysis.

The thermomechanical simulator was used to perform heat treatments at different austempering temperatures and times. The heat treatment cycle was as follows: The samples were heated at a rate of 10 °C s^{-1} up to austenitising temperature of 950°C and held there for 15 min for homogenised samples, and for 30 min for non-homogenised samples. The cooling rate used from the austenitising temperature (950°C) to the austempering temperature was 100 °C s^{-1}. Isothermal treatment range was 250-450°C for different austempering times.

The presence of silicon in the range of 2-3 wt% which is common in ductile irons, significantly alters the Fe-C equilibrium diagram and its critical temperatures. It is then important to show that the austenitising temperature used in experiments falls within the austenite+Graphite region for the present ductile iron Fig. 2.3.

2.4 Hardness measurements

A Vickers hardness testing machine with 10 kg load and $\frac{2}{3}''$ objective was used to measure the macrohardness of the ductile iron as cast, and all austempered samples. The

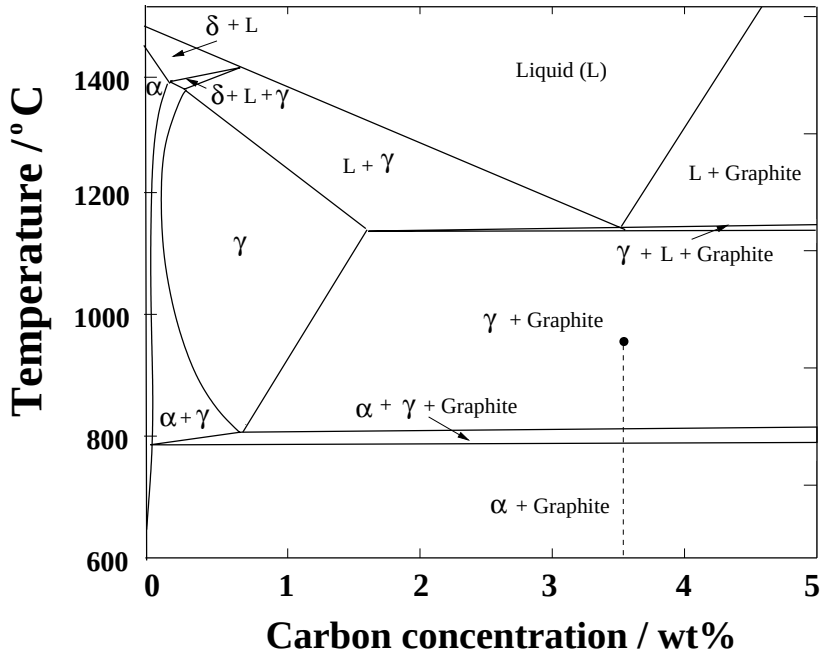

Figure 2.3: Phase diagram for Fe-C-2.5Si wt%. Calculated using MTDATA [1]. The spont in the γ + Graphite field corresponds to the austenitising temperature for the ductile iron used in experiments.

load was applied for 15 seconds during testing. Seven measurements were taken over the metallographic specimen area.

2.5 Optical microscopy

After heat treatment the samples were prepared for metallographic analysis. From each specimen a slice of 6 mm length was cut and mounted in Bakelite. The newly formed surface was ground on SiC paper to 800 grit and polished with 1 μm cloth coated with diamond paste. The samples were etched using 2% nital (2% concentrated nitric acid in methanol solution). Optical micrographs were taken with a 35 mm camera attached to a *Leitz* microscope.

2.6 Transmission electron microscopy

Specimens for transmission electron microscopy (TEM) were prepared from selected samples using both ion-milling of thin foils and the carbon extraction replica technique.

2.6.1 Thin foil preparation

3 mm diameter discs 0.5 mm thick were mechanically polished using 800 grit silicon carbide paper to 100μ thickness. Then a precision dimple grinder instrument was used to reduce the thickness to about 30μ at the centre of the discs. Finally ion-milling with two argon-ion guns was used for about 35 h, until a hole was observed. The angle between the ion beams and specimen was set to 10°. Ion milling was used instead of electropolishing, because of the extremely large difference in the electrochemical properties between graphite and the matrix. Transmission electron microscopy was conducted using a Jeol JEM-200CX electron microscope operated at 200 kV.

2.6.2 Extraction replica preparation

The extraction replica technique is very useful for identification of carbide or precipitate phases in a metallic system. The main advantage of replicas over thin foil specimens is that they eliminate any effect due to the iron matrix and thus enable the chemical composition of the carbides to be determined more accurately. Working with a ferromagnetic specimen is also more difficult in the electron microscope. The replica is very thin $\approx$ 10 nm, has no self-structure and does not burn in an electron beam.

Single-stage carbon extraction replicas were prepared using the method described by Brandon [2] from surfaces prepared as for optical microscopy but using the SPEED etching (selective etching by electrolytic dissolution) method to remove the matrix around the carbides [3]. The non-aqueous electrolyte solution used in the SPEED process consists of 10% acetyl acetone, 1% tetramethyl-ammonium chloride and methanol. A carbon coating of 20-30 nm (color blue-brown was deposited in a vacuum of 10^{-5} torr on the etched specimens. The coated surfaces were then cut with a razor blade into 3 mm squares. The replicas were etched free from the specimens with a solution of 20% nitric acid in ethanol and were captured on 400 square mesh copper grids for examination in the TEM. Fig. 2.4 shows schematically the method for making carbon extraction replica.

The extracted carbon replicas were examined using a Jeol JEM-200CX electron microscope operated at 200 kV.

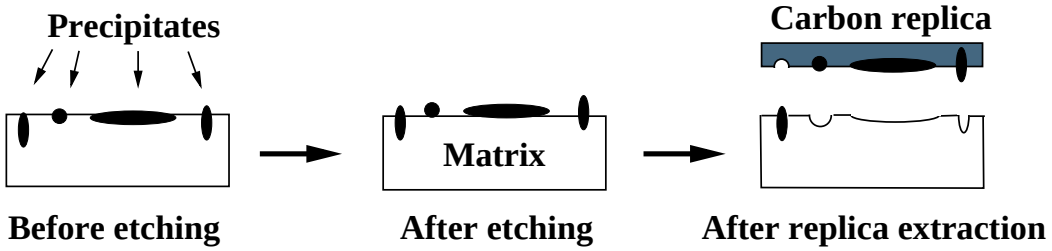

Figure 2.4: Schematic diagram illustrating the preparation of carbon replicas

2.6.3 Camera constant

A TEM consists of electromagnetic lenses which amongst other things control the magnification of the diffraction patterns. The magnification of diffraction patterns in TEM are expressed as camera length, as shown in Fig. 2.5.
The camera constant is expressed as;

$$Rd_{hkl} = L\lambda = \text{Camera constant} \tag{2.1}$$

where R is the real distance between transmitted spot and the diffracted spot, L is the camera length, d_{hkl} is the spacing of the $\{hkl\}$ crystallographic planes and λ is calculated using following equation;

$$\lambda = \frac{h}{\sqrt{2meV(1+\frac{eV}{2mc^2})}} \qquad (\mathring{A}) \tag{2.2}$$

where h is Plank's constant, m and e are the electron mass and charge respectively, V is the accelerating voltage of the electrons and c is the speed of light in vacuum.

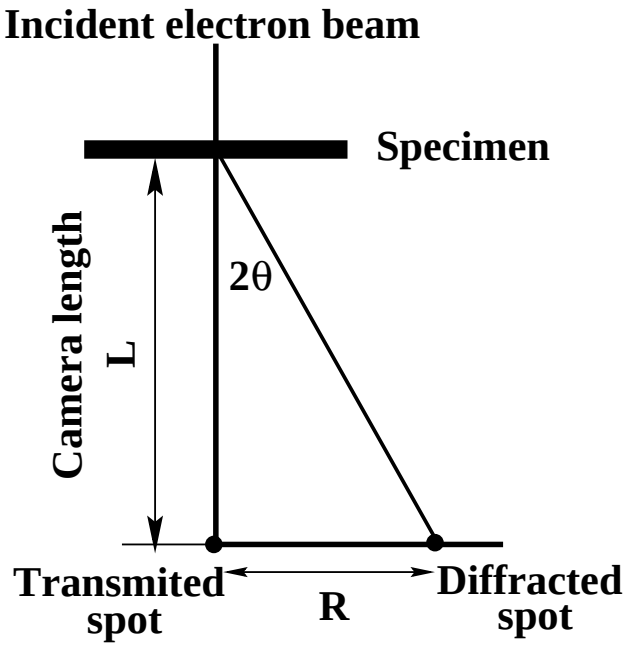

Figure 2.5: Schematic diagram showing the magnification of a diffraction pattern by electron microscopic lenses.

The camera constant was measured by examination of diffraction pattern from sputtered gold on copper grid at 200 kV on JEOL 200CX TEM. For a given electron beam direction a number of particles are oriented so as to satisfy the Bragg equation [4] hence each plane gives number of reflections lying in a cone of angle 4θ. The final diffraction

pattern contains a number of concentric rings corresponding to the $\{hkl\}$ planes which are diffracting, Fig 2.6.

To calculate the camera constant, the diameters of the rings in the diffraction pattern were measured, then the ratio between the squares of the radii of the outer rings to those of the first or second low–index ring were calculated. This enables the N values corresponding to each of the rings to be found using equation 2.3.

$$N^2 = h^2 + k^2 + l^2 \tag{2.3}$$

where h, k *and* l are the plane indices. Then d–spacings were calculated using equation 2.4 for cubic systems.

$$d = \frac{a}{\sqrt{N}} \tag{2.4}$$

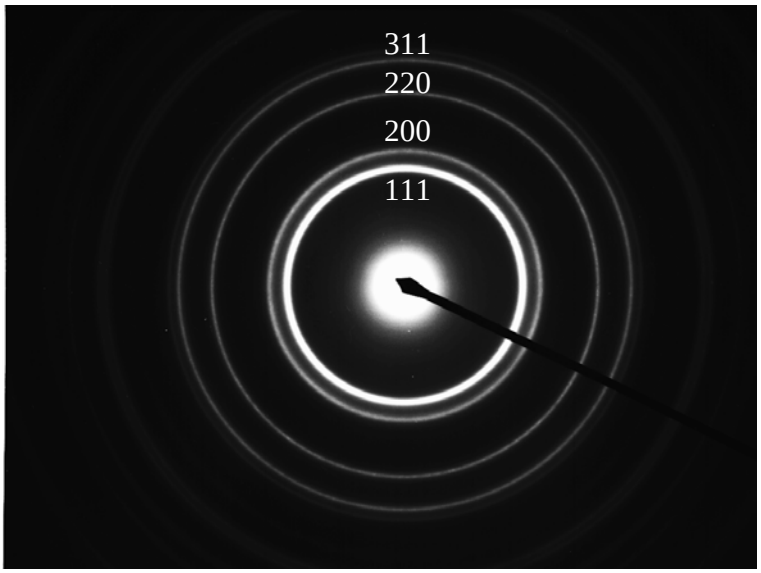

Figure 2.6: Diffraction pattern from the sputtered gold film used to determine the camera constant at 137 cm camera length (L) and 200 kV.

The accurate lattice parameter (a) of gold is 4.0780 [5] and the calculated d–spacings are shown in Table 2.1. The calculated camera constants at different camera lengths at 200k kV are shown in Table 2.2.

When ever was possible, calibration of the camera length was made using the lattice parameter of ferrite.

2.7 X-ray diffraction

The carbon content of retained austenite (x_γ), and its volume fraction (V_γ) in the austempered specimens were measured using X-ray diffraction with Cu K_α radiation at 40 kV

$\sqrt{h^2+k^2+l^2}$	Lattice spacing (d) in Å
1	2.355
2	2.039
3	1.442
4	1.230
5	1.177
6	1.096
7	0.935
8	0.912
9	0.832

Table 2.1: The calculated d–spacing in gold.

Camera length / cm	Calculated camera constant / 10^{-12} m^2
82	2.00
137	3.36
205	5.18

Table 2.2: Calculated camera constants for a number of different camera lengths at electron accelerating voltage of 200 kV.

and 40 mA. A Phillips diffractometer was used with step scan mode to cover the angular 2θ range from 47.0 to 103°. The 2θ step size was 0.03° with a dwell time of 30 s. The samples were ground and polished using the normal metallographic preparation procedure with at least two cycles of polishing and etching before the X-ray diffraction to remove any deformed layer caused by the ginding.

The volume fraction of retained austenite could be estimated from measurements of the integrated intensities of ferrite and austenite phases assuming they are the only phases present. The ratio of the intensities of diffraction peaks from two phases of a polycrystalline sample is given by Cullity [6]:

$$\frac{I_{\gamma(hkl)}}{I_{\alpha(hkl)}} = \frac{R_{\gamma(hkl)}}{R_{\alpha(hkl)}} \times \frac{V_\gamma}{V_\alpha} \tag{2.5}$$

where

$I_{\gamma(hkl)}$ = integrated intensity from a given (hkl) from the γ phase,

$I_{\alpha(hkl)}$ = integrated intensity from a given (hkl) of ferrite,

V_γ = volume fraction of γ,

V_α = volume fraction of α,

and $R_{\gamma(hkl)}$ and $R_{\alpha(hkl)}$ are given by the expression for a specific peak:

$$R = \frac{1}{v^2}[|F|^2(p)(L_p)]e^{-2m} \tag{2.6}$$

where

v = volume of unit cell,

F = structure factor,

p = multiplicity factor,

L_p = Lorentz-polarization factor,

e^{-2m} = temperature factor.

Considering that all materials in reality always exhibit a preferred orientation to some extent, it has been taken into account the average integrated intensity for at least three specific reflections for austenite and three for ferrite (Table 2.3).

Phase i	**Diffracting plane** hkl
Ferrite 1	002
Ferrite 2	112
Ferrite 3	022
Austenite 1	002
Austenite 2	022
Austenite 3	113

Table 2.3: Diffraction hkl planes used for bainitic ferrite and austenite in ADI

$$\frac{I_\gamma}{R_\gamma} = \frac{1}{3}\sum_{i=1}^{3}\frac{I_i^\gamma}{R_i^\gamma} \tag{2.7}$$

$$\frac{I_\alpha}{R_\alpha} = \frac{1}{3}\sum_{i=1}^{3}\frac{I_i^\alpha}{R_i^\alpha} \tag{2.8}$$

The value of V_γ/V_α in equation 2.5 can be obtained from the measurement of I_γ/I_α and the calculation of R_γ/R_α. Once V_γ/V_α is found, the value of V_γ can be obtained from the additional relationship.

$$V_\gamma + V_\alpha = 1 \tag{2.9}$$

The carbon concentration was calculated from the measured lattice parameter of the retained austenite. The 2θ values for three austenite peaks were used to calculate the d spacings with Bragg's law and then the lattice parameters a. These values were plotted against $\sin^2\theta$. An accurate value of a_γ is found by extrapolation to $\sin^2\theta$=1 [6]. The carbon content was then computed using the relationship developed by Dyson and Holmes [7], in which the elements are given in wt% and a_γ is given in $\mathring{A}$:

$$a_\gamma = 3.578 + 0.033C + 0.00095Mn - 0.0002Ni + 0.0006Cr$$
$$+0.0220N + 0.0056Al - 0.0004Co + 0.0015Cu + 0.0031Mo$$
$$+0.0051Nb + 0.0039Ti + 0.0018V + 0.0018W \quad (2.10)$$

References

[1] MTDATA. Metallurgical and thermochemical databank. Technical report, National Physical Laboratory, Teddington, U. K., 1989.

[2] Brandon D. G. *Modern techniques in Metallography.* Butterworths & Co. (publishers) Ltd, 1966.

[3] Ahmadabadi M. N. Eutectic carbide formation in hig mn ductile iron. *Cast Metals*, 4:182–188, 1994.

[4] Williams D. B. and Carter C. B. *Transmission Electron Microscopy II: Diffraction.* Plenum Press, New York, 1996.

[5] Barret C. S. and Massalski T. B. *Structure of Metals and Alloys.* McGraw-hill, New York, 1968.

[6] Cullity B. D. *Elements of X-ray diffraction.* Reading, MA, Addison-Wesley, 1978.

[7] Dyson D. J. and Holmes B. Effect of alloying additions on the lattice parameter of austenite. *Journal of the Iron and Steel Institute*, pages 469–474, 1970.